Carbon 103 (2016) 436–448

Contents lists available at ScienceDirect

Carbon

journal homepage: www.elsevier.com/locate/carbon

Carbon black and fumed alumina exhibiting high interface-derived mechanical energy dissipation

Yoshihiro Takizawa [1], Daojun Wang, D.D.L. Chung*

Composite Materials Research Laboratory, University at Buffalo, State University of New York, Buffalo, NY 14260-4400, USA

ARTICLE INFO

Article history:
Received 10 January 2016
Received in revised form
14 March 2016
Accepted 15 March 2016
Available online 21 March 2016

ABSTRACT

High interface-derived dissipation has been discovered by instrumented indentation in carbon black and fumed alumina. Both materials comprise nanoparticle aggregates that interlock mechanically upon compaction without a binder. The high dissipation is attributed to the high deformability and the abundance of interfaces. Compared to carbon black, similarly 600-kPa compacted 100-mN maximum-load tested fumed alumina gives lower dissipation (2.1 vs. 4.1 μJ, both values being higher than the highest previously reported value for any material, 0.175 μJ for dental enamel), lower maximum displacement (72 vs. 134 μm), higher fraction of displacement that is permanent (0.74 vs. 0.59), higher modulus (41 vs. 7 MPa), higher fractional dissipation (0.80 vs. 0.70), and lower solid content (12 vs. 18 vol.%). These differences are attributed to the greater compressibility of carbon black. The relative movement of the particles of carbon black or the graphite layers of exfoliated graphite becomes less reversible as the degree of compaction increases. Microwave-exfoliated graphite (5.25-MPa compacted, 37 vol.% solid) gives lower dissipation (1.0 μJ) and higher modulus than carbon black or fumed alumina. Furnace-exfoliated graphite (5.25-MPa compacted, 43 vol.% solid) gives even less dissipation than microwave-exfoliated graphite, due to its greater compressibility and consequent greater deformation reversibility.

1. Introduction

The dissipation of mechanical energy occurs when the stress–strain curve during loading does not overlap with that during unloading. The area between these two curves gives the dissipated energy (i.e., the energy loss) per unit volume. The energy loss involves the conversion of mechanical energy to another form of energy, which is commonly heat. Energy dissipation is not the same as the toughness, which refers to the mechanical energy input (per unit volume) needed to deform a material up to fracture.

Mechanical energy dissipation is important for passive vibration damping and sound absorption. Vibration damping is needed for essentially all structures, including wind turbines, airframe, cars, buildings, helmets, ski boards, etc. Sound absorption is needed to alleviate the noise pollution that increasingly erodes the quality of life of most people.

Mechanical energy dissipation requires a degree of viscous character in the material. The viscous character is commonly provided by bulk viscous deformation, as in the case of rubber and other polymers. However, an unconventional mechanism for providing viscous behavior is dynamic low-amplitude interfacial sliding that involves friction [1,2]. This unconventional mechanism can be significant when the material has a large amount of interface area, as in the case of an appropriately nanostructured material. Conventional carbons (such as carbon fiber) and ceramics (such as alumina) that are not in the form of polymer-matrix composites are not viscoelastic. In contrast, polymers and polymer-matrix composites are viscoelastic. However, significant viscous behavior based on the interfacial mechanism has recently been reported for exfoliated graphite [1] (not a composite), with the interfacial mechanism supported by dynamic flexural testing results and analytical modeling [2].

The interfacial mechanism mentioned above is expected to be less dependent on the temperature than the conventional bulk viscous deformation mechanism. For example, in the case of

* Corresponding author.
E-mail address: ddlchung@buffalo.edu (D.D.L. Chung).
URL: http://alum.mit.edu/www/ddlchung
[1] Permanent address: Global Aqua Innovation Center, International Center for Science and Innovation, Shinshu University, 4-17-1 Wakasato, Nagano-shi, Nagano 380-8553, Japan.

http://dx.doi.org/10.1016/j.carbon.2016.03.033
0008-6223/

polymers involving the bulk viscous deformation mechanism, the viscous character depends considerably on the temperature, particularly for temperatures around the glass transition temperature. Furthermore, polymers have limited elevated temperature resistance and limited chemical resistance compared to materials such as graphite. The concept of non-polymeric materials with strong viscous character is novel and transformative.

The plastic deformation of steel is commonly used to provide energy dissipation in steel traffic barriers, which encounter high loads during automobile impact. However, there are other applications that require energy dissipation under low loads; examples include microelectronic packages, medical devices, mechatronic devices, micromachines, robots and loudspeakers.

An effective method for evaluating the mechanical energy dissipation ability of a material is instrumented indentation (nanoindentation) during loading and subsequent unloading. This method allows tests to be conducted at different locations on the same specimen, thus allowing investigation of the spatial distribution (if any) of the energy dissipation. In addition, the specimen for nanoindentation can be small, in contrast to the relatively large specimens for conventional mechanical testing (such as tensile testing) under dynamic loading. In nanoindentation, the area between the loading and unloading curves of load vs. displacement gives the dissipated energy per loading cycle. However, comparison of this quantity for various materials should be conducted either at the same maximum load or the same maximum displacement. In the following comparison of various previously reported materials, comparison was conducted for the same maximum load. Since the maximum load values differed for different pieces of prior work, scaling of the energy dissipation was conducted in the following comparison so as to compare at the same maximum load. This scaling assumes linearity between the dissipation and the maximum load. This linearity occurs when both the loading and unloading curves of load vs. displacement are linear. However, these curves deviate from linearity, so the scaling gives only approximate dissipation values.

Based on nanoindentation results, the highest energy dissipation values previously reported [3–7] are listed in Table 1. Not listed in Table 1 due to the unclear testing conditions are the following low values of the energy dissipation (listed in order of decreasing energy dissipation): (i) 22 nJ for dentin (which is the calcified tissue underneath the dental enamel and is a composite comprising hydroxyapatite and a minor proportion of an organic material, mainly collagen, such that the proportion of organic material is higher than that of enamel) [8], (ii) 5.5 nJ for nanocrystalline glass [9], (iii) 4.1 nJ for metallic glass [10], (iv) 0.2 nJ for indium tin oxide (ITO) [11] and (v) 0.1 nJ for cement [12,13]. The high value for TiN-coated steel or TiN-coated cemented carbide [3] suggests the importance of an interface such as the coating-substrate interface in contributing to the energy dissipation.

This work provides the first report of the high mechanical energy dissipation of carbon black (a nanostructured material [14]) and fumed alumina (a similarly nanostructured material [15]). The energy dissipation is up to 4.6 and 4.1 μJ for compacted carbon black and compacted fumed alumina respectively. These values are much higher than all of the abovementioned values at comparable values of the maximum load (Table 1).

Both compacted carbon black and compacted fumed alumina are in the form of aggregates of primary particles, such that the aggregates are compressible and interlock mechanically upon compaction, thereby forming a monolithic porous solid. Compacted carbon black in the absence of a binder is a viscoelastic material [14], as recently shown by dynamic mechanical testing, with its viscous character increasing and its elastic character decreasing with increasing aggregate size. The relative movement of the particles in an aggregate contributes to the viscous deformation, while the connectivity among the aggregates contributes to the stiffness [14]. However, the viscoelastic behavior of compacted fumed alumina has not been previously reported.

Because the particles in an aggregate can move relative to one another quite easily, carbon black is compressible. Because of the compressibility, carbon black spreads under compression and conforms to the topography of the sandwiching surfaces. The spreading promotes the formation of a carbon network, even though the carbon black aggregates do not form a network before the spreading. As a consequence, carbon black is highly effective as an additive for enhancing the electrical connectivity and hence the electrical conductivity of a composite comprising nonconductive particles [16]. An example involves manganese dioxide particles, which are nonconductive and are commonly used as a cathode material in batteries. Carbon black is commonly added to this electrode in order to render the electrode conductive [17,18].

The surface topographic conformability resulting from the compressibility allows carbon black to be valuable as a constituent in thermal interface materials, which are used to reduce the thermal resistance of thermal contacts [19–23]. The improvement of thermal contacts is much needed for alleviating the problem of overheating in microelectronics. In addition, the conformability makes carbon black effective as an interlaminar filler for improving the thermal conductivity of continuous carbon fiber polymer-matrix composites in the through-thickness direction [24].

Carbon black is widely used as a reinforcing filler in rubber tires [25–27]. The spreading of the carbon black during the composite material fabrication tends to cause the carbon black to develop a fibrous morphology, which promotes the reinforcing ability. The viscoelastic behavior and energy dissipation ability of carbon black is expected to contribute to these characteristics of composites containing carbon black. However, such characteristics of carbon

Table 1
Mechanical energy dissertation of various materials tested by nanoindentation at various maximum loads.

Material	Maximum load (mN)	Energy dissipation scaled to maximum load 100 mN[a] (nJ)	Ref.
TiN-coated steel or cemented carbide[b]	5000	94	[3]
Fe-18Cr-8Ni austenitic stainless steel	500	127	[4]
Nickel-tungsten alloy	400	60	[5]
Dental enamel[c]	100	175	[6]
Carbon fiber (axial)	70	34	[7]
Carbon black	100	4600	This work
Fumed alumina	100	4100	This work

[a] The scaling conducted in this work is based on the assumption of linearity between the energy dissipation and the maximum load.
[b] The TiN coating thickness of 10 μm and the maximum displacement of 4 μm indicate that the energy dissipation involves not just the coating but also the substrate and the coating-substrate interface.
[c] The dental enamel comprises crystalline hydroxyapatite and a low proportion of organic material. The organic component contributes substantially to the energy dissipation ability.

black (as opposed to polymers containing carbon black) have received little prior attention [14].

Carbon black and fumed alumina are similar in the microstructure, as both are in the form of porous aggregates of nanoparticles. Thus, they are both compressible and are thus conformable. As a result, carbon black pastes [19–23] and fumed alumina pastes [28] are excellent thermal interface materials.

Mechanical energy dissipation also relates to the rheological behavior. This behavior of organic-based carbon black paste and fumed alumina paste has been previously reported [29]. The carbon black paste exhibits double yielding (i.e., yielding occurring at two yield stresses), whereas the fumed alumina paste exhibits single yielding [29]. This is attributed to the presence of both the relative movement of the particles and the relative movement of the aggregates in compacted carbon black, and the presence of the relative movement of the aggregates with relatively little relative movement of the particles in compacted fumed alumina. The more difficult relative movement of the particles in compacted fumed alumina compared to compacted carbon black is due to the difference in chemical bonding; the bonding is polar in alumina and non-polar in carbon. The polar bonding in fumed alumina contributes to causing greater affinity between the primary particles in fumed alumina than carbon black [29]. Both the relative movement of the particles at the interface between adjacent particles in an aggregate and the relative movement of the aggregates at the interface between adjacent aggregates involve friction. Thus, the movement causes mechanical energy dissipation. The greater is the extent of movement or the frictional force, the higher is the energy dissipation. The abovementioned structural difference between carbon black and fumed alumina suggests that the viscous character and energy dissipation are more significant in compacted carbon black than compacted fumed alumina.

Exfoliated graphite refers to the cellular low-density graphite resulting from the rapid heating of intercalated graphite flakes [30]. Compacted exfoliated graphite has been shown by instrumented indentation to provide energy dissipation of up to 0.012 nJ for a maximum load of 250 μN [31]. This energy dissipation is low, at least partly because of the low value of the maximum load. In order to compare the energy dissipation of exfoliated graphite compared to carbon black and fumed alumina, it is necessary to test all three materials at the same value of the maximum load.

The objectives of this work are (i) to advance the field of mechanical energy dissipation materials, particularly in relation to dissipation that is derived from interfacial movement and the associated friction, (ii) to provide materials with extraordinarily high mechanical energy dissipation, (iii) to investigate the energy dissipation ability of compacted carbon black, and (iv) to compare the energy dissipation ability of compacted carbon black, compacted fumed alumina and compacted exfoliated graphite.

2. Experimental methods

2.1. Materials

The carbon black was Product Vulcan XC72R from Cabot Corp., Billerica, MA, U.S.A., with DBP 188 ml/100 g, average pH 7.5, specific surface area 254 m^2/g, primary particle size 30 nm, bulk density 0.09 g/cm^3, and aggregate size 36–1122 nm. The true density was 1.8 g/cm^3. The bulk density depended on the extent of pelletization, if any. This material was a furnace black, as derived from a petroleum feedstock and exhibiting a quasi-graphitic microstructure. The manufacturing process involved injecting the feedstock into a high-temperature reactor where the hydrocarbon was cracked and dehydrogenated.

The fumed alumina was Product SpectrAl 51 from Cabot Corp. It was in the untreated state and was in the form of a white fluffy powder. Its specific gravity was 3.6 at 20 °C and its melting point was about 2000 °C. The production of fumed alumina occurred in a flame, with the associated reaction [32] commonly being

$$2\ AlCl_3 + 3\ H_2 + 1.5\ O_2 \rightarrow Al_2O_3 + 6\ HCl.$$

The material exhibited specific surface area 55 m^2/g, aggregate size 100–200 nm, and Al_2O_3 content >99.8 wt.%. Moreover, it had a positive surface charge, which was probably due to the dissociation of ionogenic groups on the particle surface and/or the differential adsorption from solution of ions of different charges into the surface region during the material fabrication. The mass loss on heating was <1.5 wt.% at 105 °C. The fumed alumina consisted of a mixture of crystalline and amorphous phases, with the crystalline phases consisting of theta, delta and gamma alumina.

The exfoliated graphite (known as worms) was obtained by the rapid heating of intercalated graphite flakes, which is known as expandable flakes, as provided by Asbury Graphite Mills (Asbury, NJ, Product No. 3772) [31]. The intercalate was sulfuric acid. The intercalation compound is known as graphite bisulfate. After the intercalation process, the expandable flake (not yet exfoliated) was rinsed by the manufacturer to remove the residual surface acid. The rinsed flake was then washed by the manufacturer with an alkaline material in order to deacidify (partially neutralize) the flake. Thus, the expandable graphite supplied by the manufacturer was not high in the intercalate concentration and had little surface residue [33]. The rapid heating of the expandable flake was conducted in this work by either (i) a microwave oven in air for a period of about 45 s, or (ii) a resistance-heating furnace at 900 °C for 2 min with flowing nitrogen. The worms obtained by either exfoliation method had not been washed. The furnace method (without washing) is the original method for obtaining exfoliated graphite and is the same as the method used in prior work [31], but the microwave method is a more convenient method and has been used quite commonly in recent years [34–36]. Comparison of the exfoliated graphite made by the furnace method and the microwave method has not been previously reported. The worms made by either method were similar in morphology and were of length 2–4 mm.

A weighed amount of carbon black, fumed alumina or exfoliated graphite was compressed in a steel cylindrical mold (31.7 mm in inner diameter) with a fitted steel piston, using a pressure of ranging from 200 to 800 kPa for carbon black and fumed alumina and a pressure of 5.25 MPa for exfoliated graphite.

The density, as determined by measurement of the mass and volume, is shown in Table 2 for each combination of material (carbon black or fumed alumina) and compaction pressure. The porosity (i.e., the volume fraction of air in the compact) was obtained from the measured density. Table 2 shows that the compacted carbon black had porosity ranging from 0.80 to 0.83 while the compacted fumed alumina had porosity ranging from 0.86 to 0.91. The higher porosity of the latter is consistent with the expected lower compressibility of the fumed alumina compared to carbon black. For both material types, the higher was the compaction pressure, the slightly lower was the porosity, as expected. The compression resulted in a monolithic disc with sharp edges and pore size mainly below 50 nm. The disc was then subjected to instrumented indentation testing, with the indentation conducted on a surface in the plane of the disc.

The compaction pressure of 5.25 MPa was chosen for the exfoliated graphite because this was one of the pressures used in prior work [31]. In the present work, for the furnace-exfoliated graphite, this pressure gave a compact with density 0.97 ± 0.01 g/cm^3, i.e., 43.0 vol.% solid; for the microwave-exfoliated graphite, this pressure gave a compact with density 0.85 ± 0.01 g/cm^3, i.e., 37.0 vol.%

Table 2
Density of compacted carbon black and compacted fumed alumina prepared at various compaction pressures. Density of carbon black = 1.8 g/cm^3. Density of alumina = 3.95 g/cm^3.

Compaction pressure (kPa)	Compacted carbon black			Compacted fumed alumina		
	Density (g/cm^3)	Volume fraction		Density (g/cm^3)	Volume fraction	
		Carbon	Air		Alumina	Air
200	–	–	–	0.36 ± 0.01	0.09 ± 0.00	0.91 ± 0.00
400	0.31 ± 0.01	0.17 ± 0.00	0.83 ± 0.00	0.42 ± 0.01	0.11 ± 0.00	0.89 ± 0.00
600	0.33 ± 0.01	0.18 ± 0.00	0.82 ± 0.00	0.47 ± 0.01	0.12 ± 0.00	0.88 ± 0.00
800	0.37 ± 0.01	0.20 ± 0.00	0.80 ± 0.00	0.57 ± 0.01	0.14 ± 0.00	0.86 ± 0.00

solid. These values of the exfoliated graphite compact density are higher than the values for the compacted carbon black and compacted fumed alumina in Table 2, and are also higher that of the exfoliated graphite compact of prior work [31].

2.2. Instrumented indentation testing

Instrumented indentation testing (known as nanoindentation testing) was conducted under load control using a nanoindenter system (MTS Systems Corporation, Model XP) that included a diamond Berkovich indenter tip. This tip had a triangle-pyramidal shape and exhibited an angle of 77° between the indenter axis and each of the three side faces of the indenter tip. A high-resolution actuator was used to apply the load on the specimen surface for the purpose of forcing the indenter into the surface. The maximum load ranged from 10 to 150 mN. The load resolution was 0.05 μN. The loading rate was 1.0 μN/s. A high-resolution sensor was used to measure the penetration into the surface in real time during loading and subsequent unloading. Thus, a plot of load versus displacement was obtained for each cycle of loading and unloading. In each loading cycle, the maximum load was held for 3 s before unloading; in this period, the displacement was due to creep. The contact area under the load was obtained from this information. In this work, the indentation direction was the direction of the pressure used in forming the compact, which was the specimen. The indentation testing was conducted at ≥3 different points for each specimen in order to confirm the reproducibility of the results.

The reduced modulus, E_r, was obtained by using the equation[2]

$$E_r = \frac{S\sqrt{\pi}}{2\beta\sqrt{A}}, \quad (1)$$

where S is known as the contact stiffness, i.e., the stiffness of the indenter-specimen contact, and is given by the slope of the initial portion of the curve of load vs. displacement during unloading (Fig. 1). In Eq. (1), β is a constant that depends only on the geometry of the indenter tip ($\beta = 1.034$ for the Berkovich tip used) and A is the projected contact area. The elastic modulus E of the specimen was then obtained by using the equation

$$\frac{1}{E_r} = \frac{(1-\nu^2)}{E} + \frac{(1-\nu_i^2)}{E_i}, \quad (2)$$

where E_i and ν_i are the elastic modulus and Poisson's ratio of the indenter tip. For the diamond indenter tip used, $E_i = 1141$ GPa and $\nu_i = 0.07$. In Eq. (2), ν is the Poisson's ratio of the specimen and is taken as 0.22 and 0.18 for alumina [37] and graphite [38] respectively.

[2] http://www.msm.cam.ac.uk/mechtest/docs/XP%20User's%20Manual.pdf, p. 29, as viewed on Jan. 24, 2014.

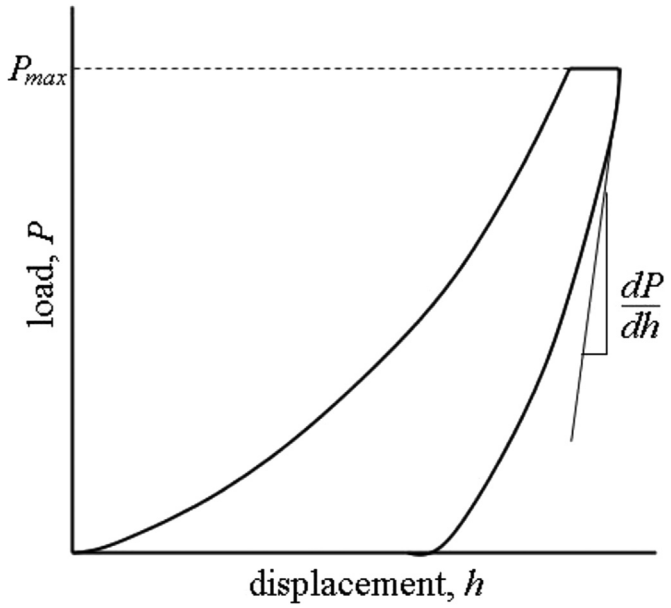

Fig. 1. Schematic illustration of the curve of load (P) vs. displacement (h) for a nanoindentation test during loading and subsequent unloading. The maximum load is P_{max}. The initial slope during unloading (dP/dh) is the contact stiffness S.

The energy dissipated in a loading cycle was given by the area between the loading and unloading curves. The input energy was given by the area under the loading curve. The fraction of input energy dissipated was given by the energy dissipated divided by the input energy.

3. Results and discussion

3.1. Carbon black

Table 3 and Fig. 2(a) show that the energy dissipation of compacted carbon black increased with increasing maximum load, as expected, due to the increase of the displacement with the load. For the same value of the maximum load, the values of the energy dissipation were similar for the compaction pressures of 400 and 600 kPa, but the value was smaller for the compaction pressure of 800 kPa. This suggests that a high degree of compaction resulted in less easy movement between the particles in carbon black. A similar effect had been previously reported for exfoliated graphite [1], the viscous character (derived from the movement of the graphite layers relative to one another) of which decreased with increasing degree of compaction of the exfoliated graphite.

Table 3 also shows that both the maximum displacement and the permanent (irreversible) displacement increased significantly with increasing maximum load, as expected. The effect of the

Table 3
Mechanical energy dissipated in a loading cycle, the fraction of input energy dissipated and the modulus at the maximum load for compacted carbon black prepared at various compaction pressures ranging from 400 to 800 kPa, as obtained by instrumented indentation at various maximum loads ranging from 10 to 100 mN.

	Compaction pressure (kPa)	Maximum load (mN)			
		10	30	50	100
Energy dissipated (nJ)	400	69 ± 0	504 ± 13	1286 ± 21	4614 ± 97
	600	73 ± 1	543 ± 22	1185 ± 49	4101 ± 198
	800	58 ± 2	383 ± 13	911 ± 13	/
Fraction of input energy dissipated	400	0.47 ± 0.01	0.59 ± 0.01	0.62 ± 0.01	0.70 ± 0.01
	600	0.50 ± 0.02	0.57 ± 0.00	0.63 ± 0.01	0.70 ± 0.00
	800	0.55 ± 0.01	0.60 ± 0.00	0.63 ± 0.00	/
Modulus at maximum load (MPa)	400	7 ± 0	6 ± 0	6 ± 0	5 ± 0
	600	7 ± 1	5 ± 0	7 ± 0	7 ± 0
	800	15 ± 1	11 ± 1	11 ± 1	/
Maximum displacement (μm)	400	31.1 ± 0.7	65.8 ± 1.0	92.0 ± 0.7	151.9 ± 1.9
	600	31.1 ± 1.0	70.3 ± 2.1	88.5 ± 3.0	133.8 ± 4.0
	800	23.6 ± 0.3	49.9 ± 1.9	68.1 ± 1.1	/
Permanent displacement (μm)	400	10.3 ± 0.5	29.3 ± 0.5	43.7 ± 1.9	75.3 ± 5.6
	600	12.1 ± 0.2	31.0 ± 0.8	41.7 ± 2.1	79.3 ± 2.4
	800	10.2 ± 0.4	23.5 ± 1.1	33.3 ± 1.2	/
Fraction of displacement that was permanent	400	0.331 ± 0.023	0.445 ± 0.001	0.475 ± 0.024	0.496 ± 0.043
	600	0.390 ± 0.019	0.442 ± 0.025	0.472 ± 0.039	0.593 ± 0.036
	800	0.433 ± 0.022	0.472 ± 0.040	0.489 ± 0.025	/

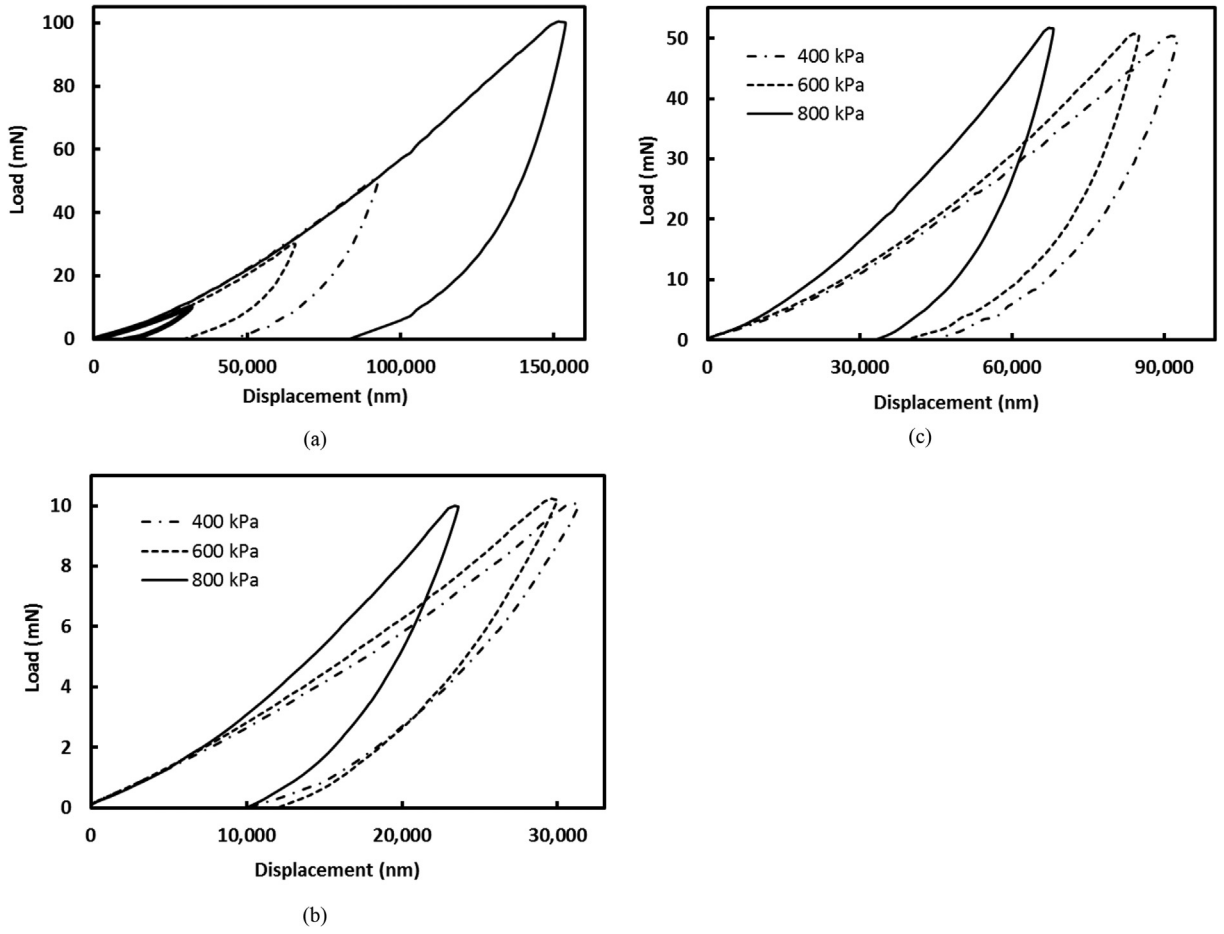

Fig. 2. The representative curves of displacement vs. load of compacted carbon black, as obtained by instrumented indentation during loading and subsequent unloading. (a) Compaction pressure of 400 kPa and various maximum indentation loads (10, 30, 50 and 100 mN). (b) Compaction pressure ranging from 400 to 800 kPa and maximum indentation load of 10 mN. (c) Compaction pressure ranging from 400 to 800 kPa and maximum indentation load of 50 mN.

compaction pressure on these quantities was small, if any. The fraction of displacement that was permanent increased with increasing maximum load for any of the three compaction pressures and tended to increase slightly with increasing compaction pressure (particularly clear for the lowest maximum load of 10 mN). This means that a higher degree of compaction, as

provided by increasing either the compaction pressure or the maximum load, caused the deformation to be less reversible. This further means that the relative movement of the particles of carbon black became less reversible as the degree of compaction increased.

For the same value of the maximum load, the values of the modulus at the maximum load were similar for the compaction pressures of 400 and 600 kPa, but the value was higher for the compaction pressure of 800 kPa (Table 3). That the modulus was higher for the higher compaction pressure is expected, due to the higher density for the higher compaction pressure.

A low value of the energy dissipation correlated with a high value of the modulus (Table 3), as expected, since a high modulus (as obtained at a high compaction pressure of 800 kPa) was associated with a low displacement (Fig. 2(b) and (c)). The fraction of input energy dissipated increased with increasing maximum load for each value of the compaction pressure, since an increase in the maximum load promoted the proportion of the deformation that was permanent (Table 3). For the same maximum load, the fraction of input energy dissipated essentially did not vary with the compaction pressure. This is consistent with the abovementioned small effect of the compaction pressure on the fraction of the deformation that was permanent.

For compacted carbon black, the highest dissipated energy of 4.6 μJ was obtained for the compaction pressure of 400 kPa and tested at the highest maximum load of 100 mN (Table 3). This corresponded to the highest value of 0.70 for the fraction of input energy dissipated. As shown in Fig. 2(a), this corresponded to a maximum displacement of 152 μm and a permanent displacement of 75 μm after unloading. This large maximum/permanent displacement contributed to causing the high energy dissipation.

3.2. Fumed alumina

Table 4 shows the results for compacted fumed alumina. For the same compaction pressure, the energy dissipation increased with increasing maximum load, as expected (Table 4 and Fig. 3(a)). For the same maximum load of 10 mN, the energy dissipation was highest, the modulus was lowest and the maximum displacement was highest for the lowest compaction pressure of 200 kPa (Table 4 and Fig. 3(b)). For the same maximum load ranging from 30 to 50 mN, the energy dissipation was highest, the modulus was lowest and the maximum displacement was highest for the compaction pressures of 200 and 400 kPa. These observations mean that a high energy dissipation correlated with a large maximum displacement, which is enabled by a low modulus, as in the case of compacted carbon black (Sec. 3.1). However, for the same maximum load of 100 mN, the energy dissipation was essentially the same for the compaction pressures of 600 and 800 kPa, while the modulus was much higher and the maximum displacement was slightly lower for 600 kPa than 800 kPa. The very low modulus (7 MPa) suggests a degree of compaction-related damage for the compaction pressure of 800 kPa.

In relation to fumed alumina for a maximum load ranging from 10 to 50 mN, in spite of the low modulus for the compaction pressure of 800 kPa compared to that of 600 kPa, the maximum displacement was slightly smaller and the energy dissipated was lower for the compaction pressure of 800 kPa than that of 600 kPa (Table 4). This suggests that the probable damage in the case of a compaction pressure of 800 kPa hindered the mechanism of energy dissipation up to a load of 50 mN. This mechanism probably mainly relates to the movement of the aggregates of fumed alumina relative to one another [25]. The larger data scatter in the energy dissipation, modulus and maximum displacement for the compaction pressure of 800 kPa compared to that of 600 kPa (Table 4) is consistent with the notion of damage in the material prepared at the high compaction pressure of 800 kPa. The extent of damage is likely different among the different points tested on the specimen surface, thus resulting in a relatively large data scatter. On the other hand, at a maximum load of 100 mN, the compaction pressures of 600 and 800 kPa gave essentially the same dissipated energy. This suggests that the higher maximum load of 100 mN reduced the abovementioned hindrance.

For compacted fumed alumina, the fraction of input energy dissipated ranged from 0.3 to 0.8 (Table 4). Among the compaction

Table 4
Mechanical energy dissipated in a loading cycle, the fraction of input energy dissipated and the modulus at the maximum load for compacted fumed alumina prepared at different compaction pressures ranging from 200 to 800 kPa, as obtained by instrumented indentation at various maximum loads ranging from 10 to 150 mN.

	Compaction pressure (kPa)	Maximum load (mN)				
		10	30	50	100	150
Energy dissipated (nJ)	200	84 ± 5	466 ± 75	993 ± 190	/	/
	400	66 ± 5	479 ± 106	871 ± 51	/	/
	600	69 ± 3	332 ± 4	628 ± 19	2118 ± 83	4095 ± 489
	800	20 ± 5	196 ± 33	383 ± 25	1660 ± 257	/
Fraction of input energy dissipated	200	0.58 ± 0.04	0.69 ± 0.03	0.75 ± 0.04	/	/
	400	0.53 ± 0.03	0.65 ± 0.12	0.44 ± 0.03	/	/
	600	0.77 ± 0.02	0.76 ± 0.04	0.75 ± 0.02	0.80 ± 0.01	0.83 ± 0.01
	800	0.34 ± 0.10	0.50 ± 0.02	0.44 ± 0.06	0.41 ± 0.03	/
Modulus at maximum load (MPa)	200	8 ± 3	11 ± 1	19 ± 1	/	/
	400	10 ± 2	10 ± 6	4 ± 0	/	/
	600	36 ± 3	33 ± 1	38 ± 2	41 ± 3	46 ± 9
	800	32 ± 5	27 ± 6	24 ± 5	7 ± 1	/
Maximum displacement (μm)	200	30.2 ± 4.2	48.4 ± 8.7	53.2 ± 4.6	/	/
	400	24.7 ± 1.9	54.3 ± 10.2	88.3 ± 6.9	/	/
	600	20.1 ± 0.3	38.2 ± 1.0	49.6 ± 1.4	72.3 ± 3.0	84.5 ± 7.6
	800	14.8 ± 0.5	26.5 ± 2.6	37.8 ± 4.6	83.9 ± 8.0	/
Permanent displacement (μm)	200	16.2 ± 1.9	27.3 ± 2.5	36.5 ± 4.7	/	/
	400	11.8 ± 1.2	32.0 ± 5.5	35.6 ± 1.0	/	/
	600	13.6 ± 0.4	27.3 ± 0.5	32.2 ± 1.0	53.3 ± 0.9	64.3 ± 5.3
	800	3.3 ± 0.4	8.1 ± 0.5	13.7 ± 1.2	26.0 ± 2.0	/
Fraction of displacement that was permanent	200	0.556 ± 0.140	0.592 ± 0.158	0.699 ± 0.149	/	/
	400	0.484 ± 0.086	0.630 ± 0.220	0.407 ± 0.043	/	/
	600	0.677 ± 0.030	0.715 ± 0.031	0.650 ± 0.038	0.739 ± 0.043	0.773 ± 0.132
	800	0.224 ± 0.034	0.310 ± 0.049	0.372 ± 0.077	0.315 ± 0.054	/

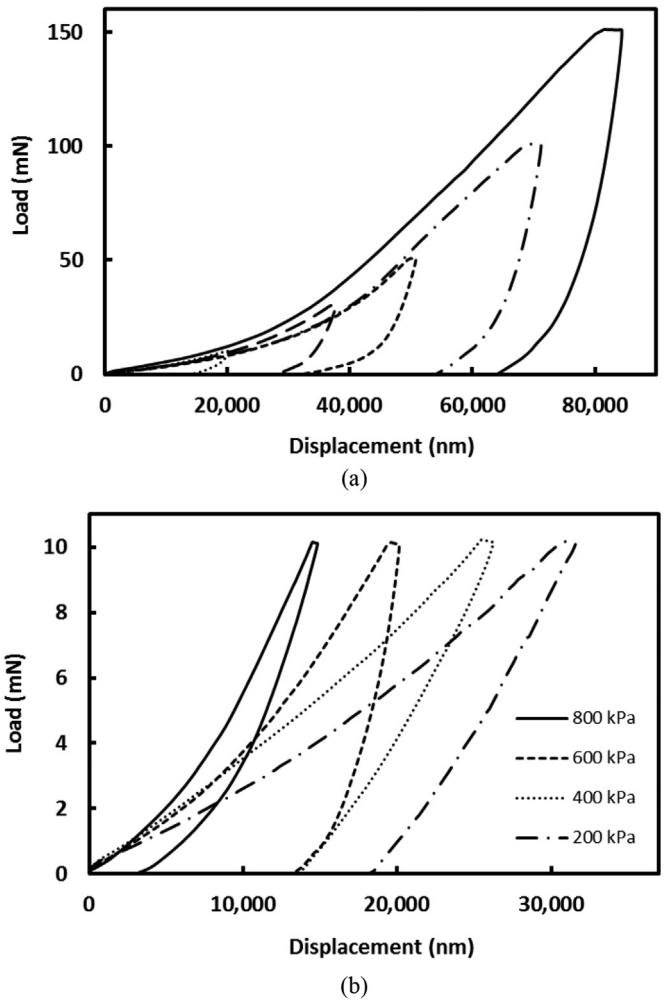

Fig. 3. The representative curves of load vs. displacement for compacted fumed alumina during loading and subsequent unloading, as obtained by instrumented indentation. (a) Compaction pressure of 600 kPa and various maximum indentation loads (10, 30, 50, 100 and 150 mN). (b) Compaction pressures ranging from 200 to 800 kPa and maximum indentation load of 10 mN.

pressures ranging from 200 to 800 kPa, this fraction tended to be highest and the modulus was highest for the intermediate compaction pressure of 600 kPa.

The fraction of input energy dissipated was considerably lower for the compaction pressure of 800 kPa than that of 600 kPa. The high energy dissipation for the case of a compaction pressure of 600 kPa corresponded to the large fraction of input energy dissipated for this compaction pressure. Furthermore, the low energy dissipation for the case of a compaction pressure of 800 kPa at a maximum load ranging from 10 to 50 mN corresponded to the small fraction of input energy dissipated for this compaction pressure. On the other hand, there was no systematic trend for the effect of the maximum load on this fraction, though this might be partly due to the large data scatter in this fraction (Table 4).

For compacted fumed alumina, the highest dissipated energy of 4.1 μJ was obtained for the compaction pressure of 600 kPa and tested at the highest maximum load of 150 mN (Table 4). This corresponded to the largest value of 0.83 for the fraction of input energy dissipated. As shown in Fig. 4(b), for the material prepared at a compaction pressure of 600 kPa and tested at a maximum load of 150 mN, the maximum displacement was 85 μm and the permanent displacement after unloading was 64 μm. This large maximum/permanent displacement contributed to causing the high energy dissipation. The second highest dissipated energy was 2.1 μJ, as obtained for this material at a maximum load of 100 mN; this corresponded to the second largest value of 0.80 for the fraction of input energy dissipated.

3.3. Comparison of carbon black and fumed alumina

For the compacted fumed alumina, the fraction of input energy dissipated did not vary significantly with the maximum load (Table 4), in contrast to the increase of this fraction with increasing maximum load for the compacted carbon black (Table 3). This is consistent with the notion that an increase in the maximum load promoted the relative movement of the particles in compacted carbon black, whereas this increase in the maximum load essentially did not result in this promotion in case of compacted fumed alumina, due to the ionic bonding and consequent greater difficulty for the relative movement of the particles in case of compacted fumed alumina. On the other hand, the values of the fraction of input energy dissipated were comparable for the two types of material.

For a compaction pressure of 600 kPa and a maximum load of 100 mN, the fraction of input energy dissipated was 0.70 and 0.80 for compacted carbon black and compacted fumed alumina respectively. In spite of the higher fraction for the compacted fumed alumina, the dissipated energy was only 2.1 μJ (Table 4), compared to 4.1 μJ for compacted carbon black (Table 3). The higher dissipated energy for compacted carbon black was mainly due to the larger displacement. The permanent displacement was 134 μm for carbon black and was 72 μm for compacted fumed alumina; the permanent displacement after unloading was 79 μm for carbon black and was 53 μm for compacted fumed alumina (Fig. 4(a)).

For compacted fumed alumina, the highest value of the energy dissipation was 4.1 μJ (Table 4), which is below the value of 4.6 μJ for the compacted carbon black (Table 3). At the same maximum load of 100 mN, compacted carbon black gave much higher values of the energy dissipation than compacted fumed alumina (Fig. 4(a) and Tables 3 and 4). Comparison of Tables 3 and 4 also shows that the modulus is higher for compacted fumed alumina than compacted carbon black. Thus, the relatively low energy dissipation of the compacted fumed alumina compared to the compacted carbon black is attributed to the high modulus of the former.

For fumed alumina (Table 4), the fraction of the displacement that was permanent did not show a consistent systematic dependence on the compaction pressure or the maximum load, at least partly due to the large data scatter, which was larger than that for carbon black (Table 3). However, this fraction for fumed alumina was lower for the compaction pressure of 800 kPa than the lower compaction pressures (200–600 kPa). This means that, for fumed alumina, the deformation was more reversible for the high compaction pressure of 800 kPa. This behavior for the compaction pressure of 800 kPa is consistent with the low fraction of input energy dissipated for this compaction pressure. In contrast, for carbon black, the fraction of displacement that was permanent increased monotonically with increasing compaction pressure up to 800 kPa (Table 3), due to the greater difficulty of relative movement of the particles when the degree of compaction was high (in spite of the greater degree of mechanical interlocking among the particles for the high compaction pressure).

The relatively large data scatter for fumed alumina compared to carbon black is attributed to the less easy movement of the particles relative to one another for the case of fumed alumina and the consequent lower degree of smoothness of the movement. The mechanical interlocking among the particles of fumed alumina probably occurred to a greater degree at the high compaction

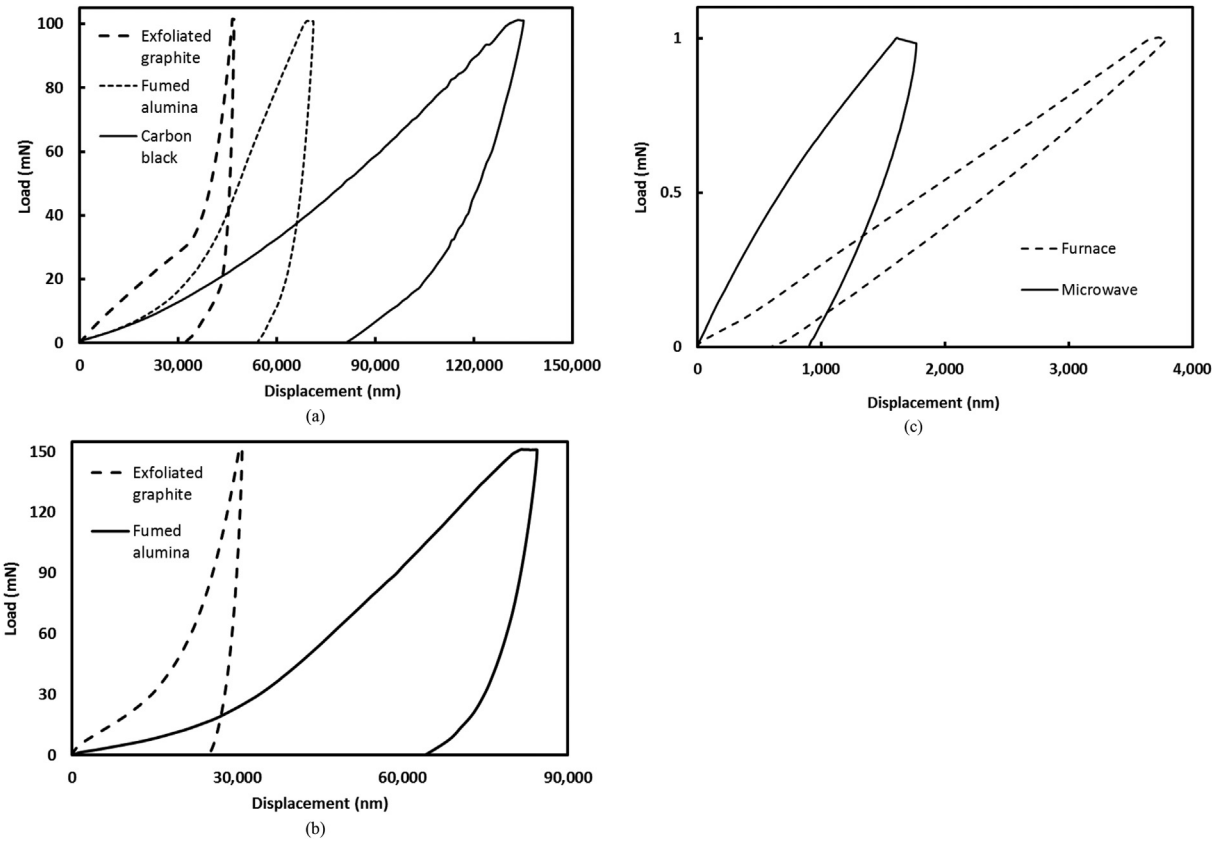

Fig. 4. Representative curves of load versus displacement during loading and subsequent unloading, as obtained by instrumented indentation, for compacted carbon black, compacted fumed alumina and compacted exfoliated graphite in comparison. (a) Compacted exfoliated graphite (microwave exfoliated, compaction pressure 5.25 MPa), compacted fumed alumina (compaction pressure 600 kPa), and compacted carbon black (compaction pressure 600 kPa), with the curves obtained at a maximum load of 100 mN. (b) Compacted microwave-exfoliated graphite (compaction pressure 5.25 MPa, dashed curve) and compacted fumed alumina (compaction pressure 600 kPa, solid curve), with the curves obtained at a maximum load of 150 mN. (c) Furnace-exfoliated graphite compact and microwave-exfoliated graphite compact, both with compaction pressure 5.25 MPa.

pressure of 800 kPa, thereby enabling the deformation to be more reversible. For compaction pressures other than 800 kPa, the fraction of displacement that was permanent ranged from 0.48 to 0.77 for fumed alumina (Table 4) and from 0.33 to 0.59 for carbon black (Table 3). This means that, for both carbon black and fumed alumina, the extent of permanent deformation and extent of reversible deformation are comparable. The permanent deformation is due to the substantial irreversible part of the compressibility of these materials, whereas the reversible deformation is due to the substantial elastic character of the compressibility of these materials. Furthermore, carbon black exhibited greater reversibility of the deformation than fumed alumina for compaction pressures other than 800 kPa. The greater reversibility for carbon black was consistent with the higher degree of mechanical interlocking among the particles for carbon black. The connectivity of the particles was necessary for the deformation to be reversible. Due to the lower degree of deformation reversibility for fumed alumina compared to carbon black, the highest value of the fraction of input energy dissipated was greater for fumed alumina (0.83) than carbon black (0.70). A greater degree of reversibility of the deformation is attractive for repeated use of the material for energy dissipation.

3.4. Exfoliated graphite

Tables 3–5 and Fig. 4(a) show a comparison among compacted microwave-exfoliated graphite, compacted carbon black and compacted fumed alumina. The energy dissipation of compacted microwave-exfoliated graphite was 1.1 μJ for a maximum load of 150 mN. This energy dissipation is much lower than the value of 4.6 μJ for compacted carbon black (tested at a lower maximum load of 100 N) and the value of 4.1 μJ for compacted fumed alumina (tested at the same maximum load of 150 mN). For the maximum load of 100 mN, the energy dissipation was 0.98, 4.61 and 2.12 μJ for compacted microwave-exfoliated graphite, carbon black and fumed alumina respectively. Hence, the energy dissipation was highest for compacted carbon black, lower for compacted fumed alumina and much lower for compacted microwave-exfoliated graphite. The exceptionally low energy dissipation of compacted microwave-exfoliated graphite was related to the exceptionally low value of the maximum displacement (which decreased with increasing maximum load) and the exceptionally high value of the modulus (which increased with increasing maximum load) (Tables 3–5). As for carbon black and fumed alumina, high energy dissipation correlated with a large maximum displacement. The decrease of the maximum displacement with the maximum load and the increase of the modulus with increasing maximum load for compacted microwave-exfoliated graphite suggest that the increased load caused additional compaction of the microwave-exfoliated graphite, thereby stiffening the compact. This notion is consistent with the previous report that commercial flexible graphite (fabricated at a compaction pressure that was much higher than those used for making compacted microwave-exfoliated graphite) gave less energy dissipation, less maximum displacement and higher modulus than compacted microwave-exfoliated graphite [31].

The high energy dissipation of compacted carbon black

Table 5
Mechanical energy dissipated in a loading cycle, the fraction of input energy dissipated and the modulus at the maximum load for compacted exfoliated graphite (microwave exfoliated, 37 vol.% solid) prepared by compaction at 5.25 MPa, as obtained by instrumented indentation at various maximum loads ranging from 0.10 to 150 mN.

Maximum load (mN)	0.10	0.25	1.00	2.50	10.0	50.0	100	150
Energy dissipated (nJ)	0.00918 ± 0.00025	0.0415 ± 0.0022	0.665 ± 0.046	5.76 ± 0.45	69.0 ± 4.1	877 ± 71	980 ± 230	1110 ± 90
Fraction of input energy dissipated	0.50 ± 0.00	0.707 ± 0.057	0.657 ± 0.020	0.630 ± 0.041	0.620 ± 0.029	0.77 ± 0.02	0.81 ± 0.01	0.83 ± 0.01
Modulus at maximum load (MPa)	/	/	220 ± 21	45 ± 17	17 ± 4	29 ± 6	224 ± 89	472 ± 65
Maximum displacement (μm)	0.327 ± 0.011	0.396 ± 0.013	1.71 ± 0.06	6.40 ± 0.77	20.6 ± 2.3	63.2 ± 3.9	46.5 ± 13.9	29.2 ± 1.8
Permanent displacement (μm)	0.127 ± 0.009	0.232 ± 0.019	0.840 ± 0.060	2.90 ± 0.08	9.80 ± 0.28	35.0 ± 2.4	31.8 ± 6.8	23.8 ± 1.4
Fraction of displacement that was permanent	0.389 ± 0.041	0.588 ± 0.067	0.493 ± 0.052	0.461 ± 0.068	0.483 ± 0.067	0.558 ± 0.072	0.799 ± 0.385	0.822 ± 0.098

compared to compacted microwave-exfoliated graphite was probably due to the greater ease of movement of the constituents in compacted carbon black than that of the constituents in compacted microwave-exfoliated graphite. The cellular structure of compacted microwave-exfoliated graphite might hinder the movement of the graphite layers in a cell wall relative to one another. In contrast, there was no cellular structure in compacted carbon black. On the other hand, the fraction of input energy dissipated was similar for compacted microwave-exfoliated graphite, compacted carbon black (600 kPa compaction pressure) and compacted fumed alumina (600 kPa compaction pressure) for a similar maximum load of 100 mN. This similarity is consistent with the notion that all three materials derived their energy dissipation from the interfacial mechanism.

An abrupt change in slope of the curve occurred at 30 mN during loading of compacted microwave-exfoliated graphite up to a maximum load of 100 mN (Fig. 4(a)). A similar change in slope occurred at 20 mN during loading of compacted microwave-exfoliated graphite up to a maximum load of 50 mN (curve not shown). However, no such abrupt change in slope occurred for compacted microwave-exfoliated graphite tested by nano-indentation in prior work up to a maximum load of only 250 μN [30]. In addition, no such abrupt change in slope occurred for compacted carbon black or compacted fumed alumina (Fig. 4(a)).

The abrupt increase in slope for compacted microwave-exfoliated graphite at 30 mN during loading to a maximum load of 100 mN was probably due to a change of the mechanism of deformation from an easy mechanism to a more difficult mechanism. An easy mechanism might possibly involve the stretching of the cell walls through the sliding of the graphite layers in the wall relative to one another, whereas a more difficult mechanism might possibly involve the sliding of the cell walls that had converged at an extremity of a cell relative to one another.

No abrupt change in slope occurred for compacted microwave-exfoliated graphite tested up to a maximum load of 150 mN (Fig. 4(b)). This might be due to the further compaction of the microwave-exfoliated graphite during loading to the high maximum load of 150 mN and the consequent gradual stiffening of the compact as loading progresses. This stiffening effect was less significant for lower values of the maximum load. The increasing stiffening at high values of the maximum load is supported by the increasing modulus (measured upon unloading at the maximum load) with increasing maximum load above 100 mN (Table 5). This trend is attributed to the increasing degree of mechanical interlocking among the worms and the consequent increasing difficulty of relative movement of the graphite layers in the exfoliated graphite as the maximum load increased. In contrast, for compacted carbon black (Table 3) and compacted fumed alumina (Table 4), the stiffening with increasing maximum load was negligible, as shown by the modulus essentially not varying with the maximum load. Due to its cellular structure, exfoliated graphite had the capacity to undergo a high degree of mechanical interlocking. In contrast, carbon black and fumed alumina did not have a cellular structure, so their capacity for mechanical interlocking was relatively small.

For microwave exfoliated graphite (Table 5), the fraction of the displacement that was permanent tended to increase with increasing maximum load. This means that the relative movement of the graphite layers in exfoliated graphite became less reversible as the maximum load increased. This is consistent with the relative movement of the particles in carbon black becoming less reversible as the maximum load increased (Table 3).

As shown in Table 6 and Fig. 4(c), compared to the furnace-exfoliated graphite compact, the microwave-exfoliated graphite compact gave greater energy dissipation (except for the lowest maximum load of 0.25 mN, for which the values were close for the two types of exfoliated graphite compact), greater fraction of input energy dissipated, higher modulus, smaller maximum displacement and greater permanent displacement (except for the lowest maximum load of 0.25 mN, for which the values were close for the two types of exfoliated graphite compact). For the same maximum load, microwave exfoliated graphite gave a higher fraction of the displacement that was permanent than furnace exfoliated graphite (Table 6). These differences between the two types of exfoliated graphite mean that the deformation was more reversible for the furnace-exfoliated graphite than the microwave-exfoliated graphite. The greater reversibility of the deformation for the furnace-exfoliated graphite resulted in a lower fraction of input energy dissipated. The greater reversibility of the deformation was associated with a lower modulus, though the lower modulus for the furnace-exfoliated graphite compact was only observed for the maximum load of 1.00 mN. A high degree of deformation reversibility of furnace-exfoliated graphite had been previously reported [31].

The two types of exfoliated graphite compact also differed in the surface morphology. The surface was smoother (more shiny) for the furnace exfoliated type than the microwave exfoliated type, as shown both visually and by microscopy (Fig. 5). This suggests a higher degree of mechanical interlocking among the worms for the furnace-exfoliated type. The higher degree of mechanical interlocking presumably resulted in greater reversibility of the deformation, as the interlocking provided the connectivity that enabled the dimensions to be restored upon unloading. On the other hand, the higher degree of interlocking did not result in a higher modulus, because the modulus is an elastic property, which does not have to relate to the elastomeric behavior [31].

Comparison of Fig. 5(a) and (c), which are for furnace-exfoliated graphite and microwave-exfoliated graphite at the same low magnification, shows that the surface is smoother, with less dark defective regions, for the former. The defective regions are graphite-deficient regions that are probably due to the local inadequate mechanical interlocking of the worms. (Such defects would

Table 6
Comparison of furnace-exfoliated graphite compact (43 vol.% solid) and microwave-exfoliated graphite compact (37 vol.% solid) in terms of the mechanical energy dissipated in a loading cycle, the fraction of input energy dissipated and the modulus at the maximum load. The compaction pressure is fixed at 5.25 MPa. The results are obtained by instrumented indentation at various maximum loads ranging from 0.25 to 10.0 mN.

Maximum load (mN)	0.25		1.00		10.0	
	Furnace exfoliated	Microwave exfoliated	Furnace exfoliated	Microwave exfoliated	Furnace exfoliated	Microwave exfoliated
Energy dissipated (nJ)	0.0462 ± 0.0044	0.0415 ± 0.0022	0.462 ± 0.004	0.665 ± 0.046	46.0 ± 8.4	69.0 ± 4.1
Fraction of input energy dissipated	0.345 ± 0.061	0.707 ± 0.057	0.242 ± 0.026	0.657 ± 0.020	0.467 ± 0.026	0.620 ± 0.029
Modulus at maximum load (MPa)	162 ± 8	/	30 ± 3	220 ± 21	14 ± 4	17 ± 4
Maximum displacement (μm)	1.03 ± 0.18	0.396 ± 0.013	3.91 ± 0.25	1.71 ± 0.06	21.3 ± 2.8	20.6 ± 2.3
Permanent displacement (μm)	0.228 ± 0.022	0.232 ± 0.019	0.603 ± 0.012	0.840 ± 0.060	6.53 ± 1.23	9.80 ± 0.28
Fraction of displacement that was permanent	0.230 ± 0.062	0.588 ± 0.067	0.155 ± 0.013	0.493 ± 0.052	0.319 ± 0.100	0.483 ± 0.067

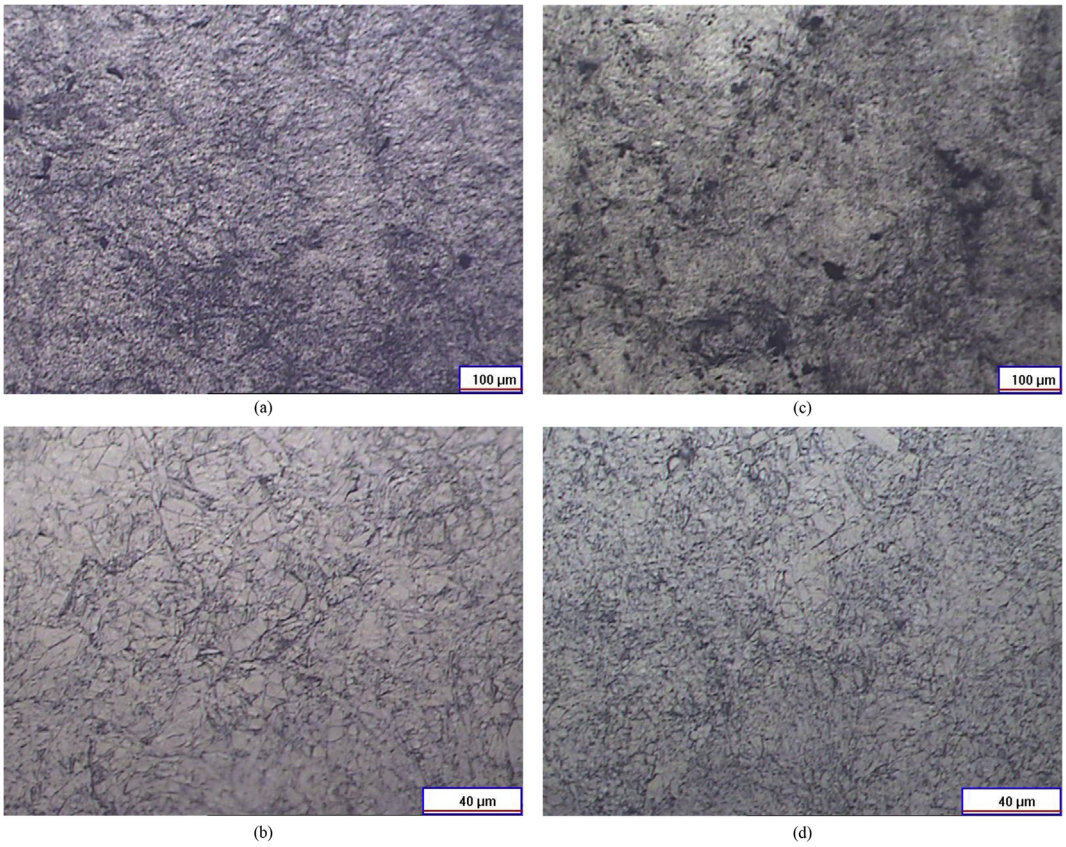

Fig. 5. Optical microscope photographs of the surface of exfoliated graphite compacts. (a) Furnace-exfoliated graphite at low magnification. (b) Furnace-exfoliated graphite at high magnification. (c) Microwave-exfoliated graphite at low magnification. (d) Microwave-exfoliated graphite at high magnification (A color version of this figure can be viewed online.).

be less if the worms have been shaken, so that they are distributed more uniformly prior to the compaction. No shaking is performed in this work.) Comparison of Fig. 5(b) and (d), which are for these two materials at the same high magnification, shows that the microstructure is coarser for the former. Both the greater smoothness and the coarser microstructure of furnace-exfoliated graphite are attributed to the higher degree of mechanical interlocking of the worms.

The scientific origin for the lower degree of interlocking for the microwave-exfoliated graphite is attributed to the observed greater difficulty for the worms to adjust their positions relative to one another during compaction. It was visually observed that the microwave-exfoliated worms were more sticky than the furnace-exfoliated worms in relation to the worms clinging to one another and the worms sticking to the compacting surfaces. Presumably, due to the relatively short time for the heating during microwave exfoliation, the amount of surface residue was greater for the microwave-exfoliated worms than the furnace-exfoliated worms, thus causing more stickiness for the former. The effect of processing on the surface characteristics of exfoliated graphite is a subject that should be investigated further.

3.5. Further discussion

Fig. 6(a) shows that, for any of the materials studied, the energy dissipated increases with increasing maximum load, as expected. For the same maximum load of 100 mN, the energy dissipated is highest for carbon black, lowest for exfoliated graphite (microwave exfoliated) and intermediate for fumed alumina. On the other hand, for the same maximum load from 10 to 100 mN, the fraction of

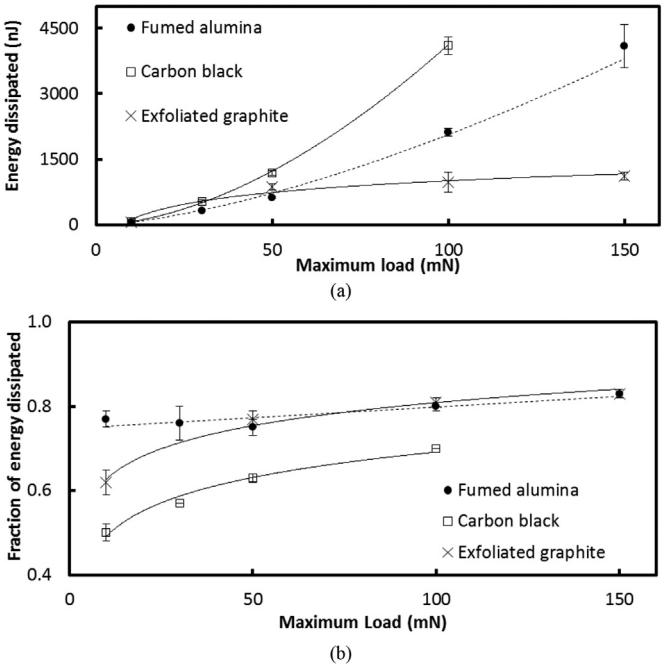

Fig. 6. Effect of the maximum load on the energy dissipation. (a) Plot of the energy dissipated vs. the maximum load. (b) The plot of the fraction of energy dissipated vs. the maximum load. Fumed alumina and carbon black were compacted at 600 kPa. Microwave-exfoliated graphite was compacted at 5.25 MPa.

input energy dissipated is lower for carbon black compared to fumed alumina or exfoliated graphite, as shown in Fig. 6(b). The high energy dissipated of carbon black (Fig. 6(a)) in spite of the low fraction of energy dissipated (Fig. 6(b)) is due to the high maximum displacement that carbon black provides. Carbon black gives the highest maximum displacement, which results in high energy dissipated (Fig. 7(a)), though carbon black gives a relatively low value of the fraction of input energy dissipated (Fig. 7(b)). Fig. 8 shows that, at the same maximum load ranging from 50 to 150 mN, the modulus is highest for exfoliated graphite, lowest for carbon black, and intermediate for fumed alumina.

Both values of 4.6 μJ (for compacted carbon black at a maximum load of 100 mN and a maximum displacement of 152 μm) and 4.1 μJ (for compacted fumed alumina at a maximum load of 150 mN and a maximum displacement of 85 μm) for the dissipated energy are extraordinarily high compared to those of prior work (as reviewed in the Introduction); the highest energy dissipation previously reported is 630 nJ (i.e., 0.63 μJ), as observed in stainless steel at a maximum load of 500 mN and a maximum displacement of 3.5 μm [4]. Even at a much higher maximum load (500 mN) than this work, stainless steel gave much lower energy dissipation (634 nJ) [4] than compacted carbon black (up to 4600 nJ) or compacted fumed alumina (up to 4100 nJ). At the low maximum load of 10 mN, the energy dissipation values of 73 nJ (for compacted carbon black) and 69 nJ (for compacted fumed alumina) for the compaction pressure of 600 kPa (Tables 3 and 4) are still high compared to the values of Ni-W, carbon fiber (axial), dentin, nanocrystalline glass, metallic glass, indium tin oxide and cement (as reviewed in the Introduction). The displacement is lower in prior work than this work.

The large strain (displacement) in the materials of this work makes the materials not suitable as a structural material, but it may be used as an energy-dissipating constituent in a structure. An example is a structure in the form of stiff face sheets sandwiching the material of this work, as obtained by compacting the carbon black or fumed alumina between the face sheets. Polymers are commonly used for this purpose, being sandwiched by stiff face sheets in a technique known as constrained layer damping [39]. However, polymers suffer from their viscoelastic properties varying considerably with the temperature [40], in addition to their inability to withstand high temperatures. In contrast, carbon and ceramics exhibit properties that are relatively independent of the temperature, in addition to being able to withstand relatively high temperatures.

It had been previously reported that carbon black as an interlaminar filler increased the through-thickness thermal conductivity of carbon fiber polymer-matrix composites [24]. However, the use of this interlaminar filler for damping enhancement had not been previously reported. On the other hand, carbon black had been used as a filler to increase slightly the temperature for a polymer to be effective for vibration damping [41,42]. Exfoliated graphite had been previously used as an interlaminar filler for damping enhancement, but its inherent porosity even after compaction was detrimental to the strength of the composite [43].

Compacted fumed alumina had recently been reported to be a

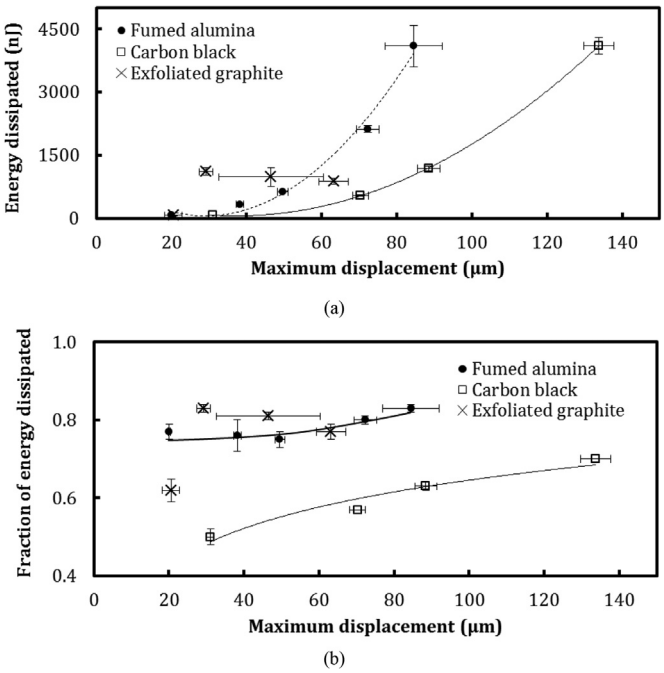

Fig. 7. The effect of the maximum displacement on the energy dissipation. (a) The plot of the energy dissipated vs. the maximum displacement. (b) The plot of the fraction of energy dissipated vs. the maximum displacement. Fumed alumina and carbon black were compacted at 600 kPa. Microwave-exfoliated graphite was compacted at 5.25 MPa.

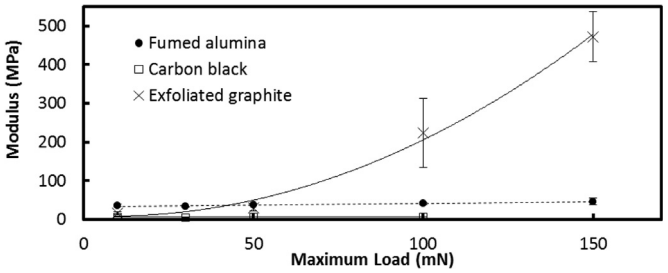

Fig. 8. The plot of the modulus vs. the maximum load. Fumed alumina and carbon black were compacted at 600 kPa. Microwave-exfoliated graphite was compacted at 5.25 MPa.

low-k dielectric material, which refers to an electrically insulating material that exhibits a low value of the relative dielectric constant, which is needed for alleviating the problem of signal propagation delay in a microelectronic package [15]. The energy dissipating ability of this material is advantageous for this application, due to the mechanical forces that microelectronics can encounter inadvertently.

4. Conclusions

Extraordinarily high energy dissipation unconventionally based on the interfacial mechanism was discovered in carbon black and fumed alumina. This unconventional mechanism is in contrast to the conventional bulk viscous deformation mechanism. The energy dissipation is greater than that of exfoliated graphite, which also derives its viscous character from the interfacial mechanism.

The extraordinarily high dissipated energy obtained for carbon black was 4.6 μJ (for 400-kPa compacted carbon black with 17 vol.% solid, tested by conducting one cycle of instrumented indentation at a maximum displacement of 152 μm and a permanent displacement of 75 μm after unloading). The extraordinarily high dissipated energy obtained for fumed alumina was lower, namely 2.1 μJ (for 600-kPa compacted fumed alumina with 12 vol.% solid, tested at a maximum displacement of 72 μm and a permanent displacement of 53 μm). Both materials were tested for a maximum load of 100 mN. Compared to carbon black, similarly 600-kPa compacted and 100-mN tested fumed alumina gave lower energy dissipation (2.1 vs. 4.1 μJ), lower maximum displacement (72 vs. 134 μm), lower permanent displacement (53 vs. 79 μm), higher fraction of displacement that is permanent (0.74 vs. 0.59), higher modulus (41 vs. 7 MPa), higher fractional energy dissipation (0.80 vs. 0.70), and lower solid content (12 vs. 18 vol.%).

For carbon black, the energy dissipation was similarly high and the modulus was similarly low (5–7 MPa) for compaction pressures of 400 and 600 kPa. For 800 kPa, the energy dissipation and displacement were lower, while the modulus was higher (11 MPa).

The higher dissipated energy for compacted carbon black compared to compacted fumed alumina was due to the larger displacement, which stemmed from the greater compressibility. The greater compressibility resulted a lower porosity in the compact and was enabled by the greater ease of relative movement of the particles. This movement was in addition to the relative movement of the aggregates. These differences between carbon black and fumed alumina are attributed to the difference in chemical bonding causing the primary particles in an aggregate to move relative to one another less easily for fumed alumina than carbon black, as supported by previously reported single yielding for alumina and double yielding for carbon black [29]. The degree of reversibility of the displacement showed more data scatter for fumed alumina than carbon black.

For carbon black and exfoliated graphite, the fraction of displacement that was permanent increased with increasing maximum load. This means that a higher degree of compaction caused the deformation to be less reversible. This further means that the relative movement of the particles of carbon black or that of the graphite layers of exfoliated graphite became less reversible as the degree of compaction increased. Carbon black exhibited greater reversibility of the deformation than fumed alumina for compaction pressures lower than 800 kPa.

Compacted exfoliated graphite exhibited much lower energy dissipation than both compacted carbon black and compacted fumed alumina, partly due to its relatively high modulus, which stemmed from the cellular structure of the worms and the consequent high capacity for mechanical interlocking upon compaction. The modulus tended to increase with increasing maximum load for exfoliated graphite, due to the increasing degree of mechanical interlocking, but was essentially independent of the maximum load for carbon black or fumed alumina, due to the relatively low capacity for mechanical interlocking.

For the same maximum load, the fraction of energy dissipated was lower for furnace-exfoliated graphite compact than microwave-exfoliated graphite compact, due to the greater degree of reversibility of the deformation for the former. The microwave-exfoliated graphite compact was less smooth and less shiny at the surface than the furnace-exfoliated graphite compact. These differences between the two types of exfoliated graphite compact are probably due to the lower compressibility of the microwave-exfoliated graphite, as shown by the higher porosity, and the consequent lower degree of mechanical interlocking. Compacted (5.25-MPa pressure) microwave-exfoliated graphite (37 vol.% solid) gave low energy dissipation (1.0 μJ, 100 mN), but high modulus (220 MPa). The energy dissipation was even lower for furnace-exfoliated graphite (43 vol.% solid), due to the greater degree of deformation reversibility. The ease of movement of the constituents in compacted carbon black was apparently greater than that of the constituents in compacted exfoliated graphite.

High dissipated energy stemmed from high maximum displacement, so it correlated with low modulus but did not correlate well with the fraction of input energy dissipated. This fraction was up to 0.83 for the materials of this work. The dissipated energy tended to decrease with increasing compaction pressure.

The high energy dissipation values obtained in this work had not been previously obtained for any material at such a low value of the maximum load. The highest value previously reported for any solid material at a maximum load of 100 mN was 0.175 μJ, which was for dental enamel [6]. The values of the energy dissipation achieved in this work for compacted carbon black, compacted fumed alumina and compacted exfoliated graphite all exceed this value. In particular, extraordinarily high energy dissipation exceeding 4 μJ was achieved in this work in compacted carbon black and compacted fumed alumina. The high values obtained for compacted carbon black and compacted fumed alumina are attributed to the large displacement and the abundance of interfaces in these materials. Slight slippage at the interfaces and the associated friction resulted in energy dissipation.

Acknowledgment

The authors are grateful to Professor Cemalettin Basaran of University at Buffalo, State University of New York, for nanoindentation-related technical assistance.

References

[1] D.D.L. Chung, Interface-derived extraordinary viscous behavior of exfoliated graphite, Carbon 68 (2014) 646–652.
[2] Y. Chen, W. Dong, Parametric studies of nonlinear damping behavior of APS thermal barrier coatings based on cohesive interface model, in: Proceedings of the ASME Turbo Expo 2012, Structures and Dynamics, Parts A and B, Vol. 7, 2012, p. 13, http://dx.doi.org/10.1115/GT2. Paper No. GT2012-69343.
[3] G.S. Fox-Rabinovich, S.C. Veldhuis, V.N. Scvortsov, L.S. Shuster, G.K. Dosbaeva, M.S. Migranov, Elastic and plastic work of indentation as a characteristic of wear behavior for cutting tools with nitride PVD coatings, Thin Solid Films 469–470 (2004) 505–512.
[4] D. Ye, S. Matsuoka, N. Nagashimaet, Determination of fatigue mesoscopic mechanical properties of an austenitic stainless steel using depth-sensing indentation (DSI) technique, Mater. Sci. Eng. A 456 (1–2) (2007) 120–129.
[5] P. Cavaliere, Mechanical properties of nanocrystalline metals and alloys studied via multi-step nanoindentation and finite element calculations, Mater. Sci. Eng. A 512 (1–2) (2009) 1–9.
[6] L.H. He, M.V. Swain, Energy absorption characterization of human enamel using nanoindentation, J. Biomed. Mater. Res. A 81 (2) (2007) 484–492.
[7] M. Hao, R. Luo, Q. Xiang, Z. Hou, W. Yang, H. Shang, Effects of fiber-type on the microstructure and mechanical properties of carbon/carbon composites, New Carbon Mater. 29 (6) (2014) 444–453.

[8] L.E. Bertassoni, M.V. Swain, Influence of hydration on nanoindentation induced energy expenditure of dentin, J. Biomech. 45 (2012) 1679–1683.
[9] K. Narita, Y. Benino, T. Fujiwara, T. Komatsu, Vickers nanoindentation hardness and deformation energy of transparent erbium tellurite nanocrystallized glasses, J. Non-Cryst. Solids 316 (2003) 407–412.
[10] K. Wang, D. Pan, M.W. Chen, W. Zhang, X.M. Wang, A. Inoue, Measuring elastic energy density of bulk metallic glasses by nanoindentation, Mater. Trans. 47 (8) (2006) 1981–1984.
[11] M.S. Pradeepkumar, K.P. Sibin, N. Swain, N. Sridhara, A. Dey, H.C. Barshilia, A.K. Sharma, Nanoindentation response of ITO film, Ceram. Int. 41 (2015) 8223–8229.
[12] M.R. Taha, E. Soliman, M. Sheyka, A. Reinhardt, M. Al-Haik, Fracture toughness of hydrated cement paste using nanoindentation, in: B.H. Oh, et al. (Eds.), Fracture Mechanics of Concrete and Concrete Structures – Recent Advances in Fracture Mechanics of Concrete, Korea Concrete Institute, Seoul, 2010, pp. 105–111. Proceedings of FraMCoS-7, May 23-28, 2010.
[13] K.K. Jha, N. Suksawang, D. Lahiri, A. Agarwal, Energy-based analysis of nanoindentation curves for cementitious materials, ACI Mater. J. 109 (1) (2012) 81–90.
[14] S. Lu, D.D.L. Chung, Viscoelastic behavior of carbon black and its relationship with the aggregate size, Carbon 60 (2013) 346–355.
[15] Y. Takizawa, D.D.L. Chung, Fumed-alumina-derived nanoporous alumina as a new low-k dielectric material for microelectronic packaging, J. Electron. Mater. 44 (7) (2015) 2211–2220.
[16] H. Yazdani, K. Hatami, E. Khosravi, K. Harper, B.P. Grady, Strain-sensitive conductivity of carbon black-filled PVC composites subjected to cyclic loading, Carbon 79 (2014) 393–405.
[17] C.A. Frysz, S. Xiaoping, D.D.L. Chung, Carbon filaments and carbon black as a conductive additive to the manganese dioxide cathode of a lithium electrolytic cell, J. Power Sources 58 (1) (1996) 41–54.
[18] M. Moalleminejad, D.D.L. Chung, Dielectric constant and electrical conductivity of carbon black as an electrically conductive additive in a manganese-dioxide electrochemical electrode, and their dependence on electrolyte permeation, Carbon 91 (2015) 76–87.
[19] C. Chia-Ken Leong, D.D.L. Chung, Carbon black dispersions and carbon-silver combinations as thermal pastes that surpass commercial silver and ceramic pastes in providing high thermal contact conductance, Carbon 42 (11) (2004) 2323–2327.
[20] C. Leong, Y. Aoyagi, D.D.L. Chung, Carbon black pastes as coatings for improving thermal gap-filling materials, Carbon 44 (3) (2006) 435–440.
[21] C. Lin, D.D.L. Chung, Graphite nanopletelet pastes versus carbon black pastes as thermal interface materials, Carbon 47 (1) (2009) 295–305.
[22] K. Hu, D.D.L. Chung, Flexible graphite modified by carbon black paste for use as a thermal interface material, Carbon 49 (2011) 1075–1086.
[23] C. Lin, D.D.L. Chung, Effect of carbon black structure on the effectiveness of carbon black thermal interface pastes, Carbon 45 (15) (2007) 2922–2931.
[24] H. Han, J.T. Lin, Y. Aoyagi, D.D.L. Chung, Enhancing the thermal conductivity and compressive modulus of carbon fiber polymer-matrix composites in the through-thickness direction by nanostructuring the interlaminar interface with carbon black, Carbon 46 (7) (2008) 1060–1071.
[25] A. Mostafa, A. Abouel-Kasem, M.R. Bayoumi, M.G. El-Sebaie, Rubber-filler interactions and its effect in rheological and mechanical properties of filled compounds, J. Test. Eval. 38 (3) (2010) 347–359.
[26] M. Gerspacher, C.P. O'Farrell, Carbon Black-elastomer Composites, in: Chemistry and Physics of Network Formation, vol. 49, Education Symposium - American Chemical Society, Rubber Division, 2002, pp. E1–E13.
[27] M. Gerspacher, Advanced CB characterizations to better understand polymer-filler interaction. A critical survey, KGK, Kautsch. Gummi Kunstst. 62 (5) (2009) no pp. given.
[28] C. Lin, D.D.L. Chung, Nanostructured fumed metal oxides for thermal interface pastes, J. Mater Sci. 42 (22) (2007) 9245–9255.
[29] C. Lin, D.D.L. Chung, Rheological behavior of thermal interface pastes, J. Electron. Mater 38 (10) (2009) 2069–2084.
[30] D.D.L. Chung, A review of exfoliated graphite, J. Mater. Sci. 51 (2016) 554–568.
[31] P. Chen, D.D.L. Chung, Elastomeric behavior of exfoliated graphite, as shown by instrumented indentation testing, Carbon 81 (2015) 505–513.
[32] P. Somasundaran, Encyclopedia of Surface and Colloid Science, second ed., vol. 7, CRC Press, Boca Raton, FL, 2006, p. 5317.
[33] X. Hong, D.D.L. Chung, Exfoliated graphite with relative dielectric constant reaching 360, obtained by exfoliation of acid-intercalated graphite flakes without subsequent removal of the residual acidity, Carbon 91 (2015) 1–10.
[34] K. Yu, Preparation of exfoliated graphite by microwave using natural graphite with different particle sizes, Adv. Mater. Res. (Zuerich Switz.) 163–167 (Pt. 3) (2011) 2333–2336. Advances in Structures.
[35] Q. Zhao, X. Cheng, J. Wu, X. Yu, Sulfur-free exfoliated graphite with large exfoliated volume: preparation, characterization and its adsorption performance, J. Ind. Eng. Chem. (Amst. Neth.) 20 (6) (2014) 4028–4032.
[36] Nagaraju Sykam, Kamal K. Kar, Rapid synthesis of exfoliated graphite by microwave irradiation and oil sorption studies, Mater. Lett. 117 (2014) 150–152.
[37] R. Tilley, Understanding Solids: the Science of Materials, John Wiley & Sons, 2005, pp. 301–302.
[38] B.T. Kelly, Physics of Graphite, Applied Science Publishers, London, 1981, pp. 43–44.
[39] P.P. Hujare, A.D. Sahasrabudhe, Experimental investigation of damping performance of viscoelastic material using constrained layer damping treatment, Proced. Mater. Sci. 5 (2014) 726–733.
[40] M. Segiet, D.D.L. Chung, Discontinuous surface-treated submicron-diameter carbon filaments as an interlaminar filler in carbon fiber polymer-matrix composites for vibration reduction, Compos. Interfaces 7 (4) (2000) 257–276.
[41] D. Shamir, A. Siegmann, M. Narkis, Vibration damping and electrical conductivity of styrene–butyl acrylate random copolymers filled with carbon black, J. Appl. Polym. Sci. 115 (4) (2010) 1922–1928.
[42] Y. Zhao, D. Liu, S. Lin, Binjian, Y. Zhao, S. Liao, Effect of the purple carbon black on the properties of NR/BR blend, IOP Conf. Ser. Mater. Sci. Eng. 62 (2014) 12033/1–12033/6. Global Conference on Polymer and Composite Materials.
[43] S. Han, D.D.L. Chung, Mechanical energy dissipation using carbon fiber polymer-matrix structural composites with filler incorporation, J. Mater. Sci. 47 (2012) 2434–2453.